Is There Really a Size effect on the Surface Energy of Nanoparticles ?

Hakim Amara, Jaysen Nelayah, Jérôme Creuze, Adrian Chmielewski, Damien Alloyeau, Christian Ricolleau, Bernard Legrand

Is There Really a Size effect on the Surface Energy of Nanoparticles ?

Hakim Amara,[1,2,*] Jaysen Nelayah,[2] Jérôme Creuze,[3] Adrian Chmielewski,[2]
Damien Alloyeau,[2] Christian Ricolleau,[2] and Bernard Legrand[4]

[1] *Laboratoire d'Etude des Microstructures, ONERA-CNRS, UMR104, Université Paris-Saclay, BP 72, Châtillon Cedex, 92322, France*
[2] *Université de Paris, Laboratoire Matériaux et Phénomènes Quantiques (MPQ), F-75013, Paris, France*
[3] *ICMMO, Université Paris Saclay, UMR 8182, Bât. 410, F-91405 Orsay Cedex, France*
[4] *Université Paris-Saclay, CEA, Service de Recherches de Métallurgie Physique, 91191 Gif-sur-Yvette, France*

Surface energy is a key quantity that controls many physical properties of materials, yet determining its value at the nanoscale remains challenging. By using N-body interatomic potentials and performing analytical calculations, we develop a robust approach to determine the surface energy of metallic nanoparticles as a function of particle size and temperature. A strong increase in the surface energy is obtained when the size of the nanoparticle decreases, both in the solid and liquid states. However, we show how the use of the classical spherical approximation to characterise the surface area of a nanoparticle leads to an almost constant surface energy with size as usually done to characterize the thermodynamic and kinetic properties of NPs in many works. We then propose a correction of the spherical approximation that is particularly useful for small size nanoparticles to improve the different models developed in the literature so far.

Surface energy (γ) is an important descriptor of metallic nanoparticles (NPs) as it drives, among others, their nucleation-growth mechanism, 3D morphology, reactivity in various environments, surface segregation,... [1]. To characterize these wide range of phenomena, the main theories developed in the literature are derived from models that involve surface energies of infinite systems [2]. In other words, γ is basically assumed to be size-independent. With this assumption, it is then possible to remarkably predict the equilibrium shape of free and supported crystallites based respectively on the Wulff and Wulff-Kaishew relations at the nanoscale [3–5]. Other examples illustrating the success of such a choice include understanding Ostwald's ripening during particle synthesis or annealing [6, 7] and the reactivity of different metal facets to gas environments in catalytic processes [8]. From a fundamental point of view, this is very surprising because it is well-known, both experimentally and theoretically, that many properties (thermodynamic, optical, mechanical, ...) of nanomaterials are strongly different from their bulk counterparts [9–14].

Despite the agreement of the different models employing the surface energy of the infinite system with the experimental observations, there is no direct evidence that the surface energy in case of NPs is indeed size-independent. This is a very complicated issue to be addressed since there is not any clear and straightforward answer to it at present. Experimentally, no systematic studies on measurement of surface energy as a function of size are presented due to the extreme difficulty to measure absolute surface energy of very small NPs [15, 16]. Theoretically, the existing literature contains many conflicting and contradictory results concerning the variation of the surface energy of metallic NPs with size. Actually, a simple dimensional argument is often put forward in case of solid NPs [17, 18]. According to this hypothesis, γ decreases with increasing size as the contribution of the different surface sites (vertices, edges), which are preponderant for small sizes, decreases at the expense of the facets. Although many studies agree with this trend [19, 20], other suggest an opposite tendency [21–23]. Indeed, the dimensional argument is not that simple since γ is commonly defined as an excess energy with respect to a reference energy normalised to a surface area related to the NP. All the discrepancies are mainly due to the difficulty to correctly define the reference state to characterize the excess energy resulting from the presence of a surface and in particular the definition of the considered surface area [24]. In any scenario, it can be noted that there is no direct evidence that the surface energy remains constant with the size.

In this letter, we investigate the surface energy of solid and liquid Cu NPs as a function of particle size with the aim to provide a robust γ calculation applicable to characterize the thermodynamic and kinetic properties of NPs through experimental or theoretical data. We focus on cuboctahedral NPs where an analytical study is possible, which is an asset of incomparable richness to the understanding of the numerical results. With our approach, the correlation between the effective area considered for γ calculation and its dependence on size is clearly demonstrated. ical potential with the size of the NP making its use perfectly universal and adapted to characterize the thermodynamic and kinetic properties of NPs.

We perform calculations at the atomic level for Cu NPs by using a specific N-body interatomic potential derived from the second moment approximation of the tight-binding scheme (TB-SMA) [25–27]. More details of the TB model can de found in Sec. I of the Supplemental Material. Our TB framework gives direct access to the total energy of each atom. This possibility to easily

analyze local energy distributions will be decisive in the following. The atomic interaction model is implemented in a Monte Carlo (MC) code in the canonical ensemble, based on the Metropolis algorithm, which allows to relax the structures at finite temperatures [28]. We consider cuboctahedral solid NP bounded by six squares and eight equilateral triangles which structure is constructed on the face-centered cubic (fcc) lattice, leading to the presence of outer facets of {100} and {111} orientations, respectively. From this structure, it is possible to define analytically all the sites for a given cluster size with k shells [18]. Indeed, this cluster contains 12 vertices (v), 24(k-1) atoms in edges (e), 6(k-1)^2 and 4(k-2)(k-1) atoms on {100} and {111} facets (f), respectively. Moreover, the total number of atoms $N(k)$, the surface $S(k)$ and the volume $V(k)$ are given by the following equations :

$$N(k) = \frac{10}{3}k^3 + 5k^2 + \frac{11}{3}k + 1 \quad (1)$$

$$S(k) = 2(3+\sqrt{3})(kd)^2 \quad (2)$$

$$V(k) = \frac{5\sqrt{2}}{3}(kd)^3 \quad (3)$$

where d corresponds to the equilibrium distance between first neighbors. To characterize the evolution of surface energy of solid and liquid states, calculations are done at two temperatures (T= 5 and 1500 K). Numerically, the so-called surface energy [29, 30] resulting from the creation of a surface is defined as an excess internal energy (E_{exc}) normalised to a given surface area, A:

$$\gamma(R) = \frac{E_{exc}}{A}, \quad (4)$$

where $E_{exc} = E_{NP}(R) - E_{ref}$. $E_{NP}(R)$ is the total energy of the NP of radius R where necessarily R and the number of k shells are linked. Lastly, E_{ref} is a reference energy to be defined. The calculation of $E_{NP}(R)$ is not an issue since it is a straightforward output of the MC simulations. On the contrary, E_{ref} and A are not well defined quantities. Typically the reference energy is commonly chosen as the energy of the bulk fcc in the solid state [31–33]. Regarding the surface area, its choice is not unique [24] and can strongly affect the results. To overcome this problem, we first consider the case of solid particles and then extend our approach to liquid systems.

We apply two complementary approaches to get an insightful analysis of our results. The first is to calculate the surface energy from MC simulations according to Eq. 4 where E_{NP} (R) is obtained after relaxation at 5 K. The second one consists of developing an analytical model by assuming that all excess energy is ascribed to the surface sites [17, 18]. This is made possible because all surface sites are perfectly identified. In both approaches, it is quite natural to consider A as the exact surface $S(k)$ of the cuboctahedral shape (see Eq. 12).

Furthermore, the identification of local energies within the NP turns out to be very precious to tackle the challenge of correctly defining E_{ref}. More precisely, by analyzing the energy profile along the radius of the NPs, we can clearly identify two populations, i.e. the core and surface atoms (see Sec. II of the Supplemental Material). Consequently, E_{ref} is simply the average energy of atoms identified in core position. In case of solid NP, E_{ref} is equal to -3.50 eV/at which is exactly the total energy per atom of a face centered cubic bulk Cu in our TB model. This result confirms that defining E_{ref} from the bulk system, as done in many works, is completely justified.

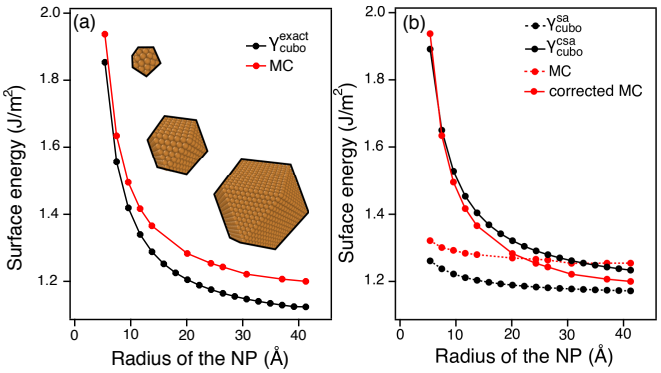

FIG. 1. Calculated surface energies for cuboctahedron Cu NPs as a function of size based on an (a) exact surface $S(k)$ and (b) a spherical (sa) approximation as well as corrected spherical approximation (csa). Both figures present analytical and MC results.

At this stage, all the quantities required to determine $\gamma(R)$ from MC simulations according to Eq. 4 are known. The calculated surface energies for the cuboctahedral Cu NP as a function of size are shown in Fig 1a. It can be seen that the surface energy decreases with particle size. More precisely, there is a significant variation for small particles (<20 Å), from 1.92 to 1.22 J/m^2. For larger particles, the decrease of γ with the size becomes negligible to reach a constant value around 1.20 J/m^2. We now consider an analytical model where the determination of $\gamma(k)$ is simply reduced to the following equation :

$$\gamma_{cubo}(k) = \frac{\sum_i n_i \gamma_i}{A}, \quad (5)$$

where γ_i represents the local excess energy for each surface sites i ($i = v, e, f$) defined as $E_i - E_{ref}$ and n_i being the number of sites of type i. In this approach, it is assumed that the excess energy is located only on the surface sites. As seen in Sec. II of the Supplemental Material, also subsurface atoms have still a slightly different energy than in bulk. We consider that they do not play a decisive role and that they can be neglected in γ calculations. In a first step, A is considered as the

exact surface $S(k)$ of the cuboctahedral NP (see Eq. 12), the related surface energy is noted $\gamma_{cubo}^{exact}(k)$. Meanwhile, the local energies of all sites (E_i) are calculated from our TB-potential for clusters of various sizes (see Sec. III of the Supplemental Material). The resulting values of γ_i are presented in Table I. From $\gamma_{cubo}^{exact}(k)$, the analytically

	γ_v	γ_e	γ_{100}	γ_{111}	$2\gamma_e - \gamma_{100} - \gamma_{111}$	$2\gamma_e - \frac{3}{2}\gamma_{100} - \frac{4}{3}\gamma_{111}$
Cu	0.94	0.62	0.43	0.37	0.44	0.09
Ag	0.60	0.38	0.28	0.22	0.26	0.05
Au	0.56	0.36	0.29	0.21	0.22	0.005

TABLE I. Local excess energy for each surface site and crucial quantities that are involved in the calculation of $\gamma_{cubo}^{exact}(k)$ and $\gamma_{cubo}^{sa}(k)$. Values are given in eV for all noble metals.

calculated surface energy for the cuboctahedral Cu NPs as a function of size is shown in Fig. 1a. Similarly to results obtained from MC simulations, the surface energy decreases strongly with size. Moreover, results from the analytical model are in good agreement with the complete MC calculations, the small difference observed being due to the the subsurface contributions. To go deeper and analyse this tendency, the first-order Taylor expansion of $\gamma_{cubo}^{exat}(k)$ turns out to be very precious (see details in Sec. IV of the Supplemental Material) :

$$\gamma_{cubo}^{exact}(k) \approx \gamma_{\infty}^{exact} + \frac{6\left[2\gamma_e - \gamma_{100} - \gamma_{111}\right]}{kd^2(3+\sqrt{3})} \qquad (6)$$

$$\gamma_{\infty}^{exact} = \frac{3\gamma_{100} + 2\gamma_{111}}{d^2(3+\sqrt{3})},$$

where γ_{∞}^{exact} corresponds to the plateau observed in Fig. 1 for large NPs (i.e. for $k \to \infty$ in Eq. 14). In addition, the second term is necessarily positive according to the γ_i hierarchy discussed above. As seen in Table I, this argument is valid for all noble metals. Consequently, the heterogeneity of the surface with different types of site explains the decrease in $\gamma(R)$, as already argued in previous works with a simple dimensional argument [17, 18].

On a purely theoretical point of view, it is quite natural to consider the true surface of the cuboctahedron $S(k)$ as done so far. Experimentally, it is however not always possible to identify the exact shape of the NP (i.e. icosahedron, decahedron, cuboctaedron,...) and even less to determine the exact surface area of the observed NPs. In practice, a spherical approximation of the different NPs to be analysed is made. Typical examples from Transmission Electron Microscope (TEM) images are presented in Fig. 2a where a radius R can be assigned to each NPs in solid states (see Sec. V of the Supplemental Material for experimental details). Within this spherical approximation, determining A of a solid NP from MC simulations is also non-trivial. Actually, the effective surface is

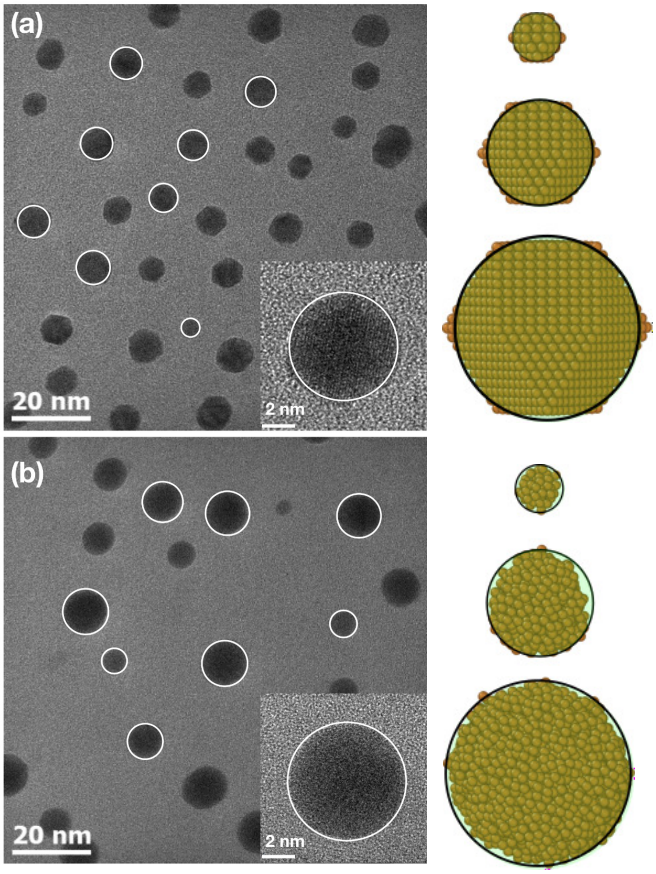

FIG. 2. Spherical approximation to determine the effective surface area from TEM images of Cu NPs in (a) solid (facetted NPs at 573 K) and (b) liquid states (non-facetted NPs with a spherical shape at 1073 K). On the right : comparison of the sphere of radius R obtained from the atomic density (ρ_∞) with configurations from MC simulations for different sizes and states of NPs containing 55 atoms, 561 atoms and 2869 atoms. For the liquid cases, it is obvious that a snapshot is not so representative of the situation since the particle is strongly deformed during the simulation.

equal to $4\pi R^2$. To address the arising difficulty in MC simulations, R is determined from the atomic density, $\rho_\infty = \sqrt{2}/d^3$, (see Sec. VI of the Supplemental Material) using the following relation : $R^3(k) = 3N(k)/4\pi\rho_\infty$. To highlight the relevance of such a choice, Fig. 2a shows the sphere obtained from ρ_∞ on snapshots of MC simulations from solid NPs, whose surface area is noted $S^{sa}(k)$. The comparison with the determination of the radius of the NPs from TEM images is clearly relevant. From Eq. 4, it is now possible to calculate the dependency with the size of the surface energy within the spherical approximation from MC simulations. As seen in Fig. 1b, the conclusion differs significantly from the exact calculation. Indeed, almost no variation is observed and γ remains rather constant around 1.23 J/m^2. Consequently, the surface energy using the spherical approximation does not depend

on the size of the system. In fact, the apparent discrepancy between the two approaches can be attributed to the different ways to calculate the surface area. Once the gap between both approaches becomes negligible, then an equivalent behaviour can be observed where the surface energy varies only slightly (see Fig. 3). Obviously, this happens for sufficiently large particles where the spherical approximation is all the more adapted. To better

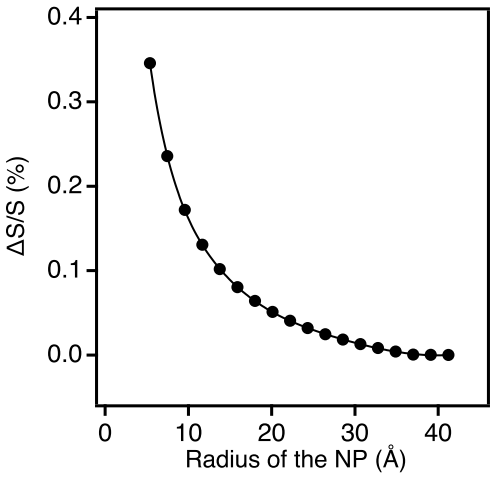

FIG. 3. Relative difference between the surface area calculated according to the spherical approximation and the exact one of the cuboctahedron as a function of size.

understand these differences with the strong decrease observed for $\gamma_{cubo}^{exact}(k)$, a first-order Taylor expansion of $\gamma(k)$ within the spherical approximation (sa), noted $\gamma_{cubo}^{sa}(k)$, is done leading to (see Sec. VII of the Supplemental Material):

$$\gamma_{cubo}^{sa}(k) \approx \gamma_{\infty}^{sa} + \frac{6\left[2\gamma_e - (3/2)\gamma_{100} - (4/3)\gamma_{111}\right]}{kd^2(25\pi)^{1/3}} \quad (7)$$

$$\gamma_{\infty}^{sa} = \frac{3\gamma_{100} + 2\gamma_{111}}{d^2(25\pi)^{1/3}}$$

As seen in Fig 1b, we confirm an almost constant variation of $\gamma(k)$ around 1.20 J/m^2. Such observation is in agreement with MC simulations where the discrepancy in the plateau is mainly due to the assumption of considering only surface sites in the analytical approach. Unfortunately, the variation of γ with size is not straightforward contrary to the exact calculation discussed previously. Indeed, nothing can be concluded about the importance of the predominant term in the numerator of Eq 17. In the particular case of Cu, it is close to zero explaining the stability of γ with size. To generalise this result, the estimation of the numerator has been extended to other noble metals (Ag and Au) confirming this trend (see Table I). Within the spherical approximation, our analytical calculations therefore suggest that the surface energy does not vary with the size and is equal to γ_{∞}^{sa} (i.e. for $k \to \infty$ in Eq. 17).

In the following, we analyse the error made in the spherical approximation where two strong assumptions were established. The first one was to determine $R(k)$ from the atomic density where all the atoms constituting the NP contribute equally. However, as seen in Sec. VI of the Supplemental Material, ρ_{∞} is correctly reproduced (at least to first order) when only considering that the surface atoms, $N_{surf}(k)$, contribute half compared to the core atoms. In the definition of $R(k)$, this is equivalent to consider that the total number of atoms is $N(k) - N_{surf}(k)/2$. In this corrected spherical approximation (csa), the surface area becomes $S^{csa}(k) = S^{sa}(1 - 1/k)$. By applying this new surface formulation to the MC simulations, a significant variation of the surface energy with the size of the NPs is found. The result (corrected MC) presented in the Fig. 1b shows a decrease for NPs smaller than 20 Å to reach a plateau in the order of 1.20 J/m^2. As seen in Fig. 1b, the same trend is observed for the analytical model, $\gamma_{cubo}^{csa}(k)$, where $S^{csa}(k)$ is considered. In other words, by using this simple surface area correction to the spherical approximation, it is possible to restore the energy dependence obtained with an exact description of the surface area. The second assumption comes from the morphology, i.e. sphere rather than cuboctahedron. Actually, the following relationship $\gamma_{cubo}^{csa}(k) \approx 1.10\gamma_{cubo}^{exact}(k)$ can be established (see Sec. VII of the Supplemental Material). Thereby, the only difference between the exact calculation and the corrected spherical approximation ones results in a morphological factor due to the difference between a sphere and a cuboctahedron. To conclude, the spherical approximation is very appropriate for large sizes (with a constant form factor) but must be corrected for small sizes by a factor modifying the radius of the NP, which itself depends on the size and takes into account the specific contribution of the surface atoms.

Let us now consider liquid NPs by applying the approach developed for solid NPs to determine E_{ref} and A in Eq. 4. For the reference energy, it is simply a question of calculating the average energy of a bulk system at 1500 K (see Sec. II of the Supplemental Material). To determine the surface area, one can no longer rely on an exact calculation. Moreover, the corrected spherical approximation allows a precise determination of this area by assuming that the number of surface atoms is very close to that in the solid state. Meanwhile, the usual spherical approximation is subject to the same disadvantage as in the solid state, i.e. an overestimation of the volume (and therefore of the radius) of the NP at small sizes, which is even greater the smaller the size is. Figure 4a shows that the variation of the surface energy with the size of the NP in the liquid state is very similar to that observed in the solid state. Thus the calculation with the usual spherical approximation shows a constant surface

energy close to 1.15 J/m^2 , whereas the corrected spherical approximation gives a strong increase of γ when the size decreases, a variation slightly higher than that observed in the solid state. This significant variation may seem very surprising if we refer to the solid state where the weight of highly energetic sites (edges and vertices) decreases in favour of that of the facets when the size increases. However, vertices, edges and facets no longer exist in the liquid state and it is tempting to think that the surface energy distribution is relatively homogeneous. To address this issue, we determined the local energies in terms of spatial distribution in the liquid state. As seen in Fig. 4b, we show the local energies for two NP sizes (561 and 5083 atoms). The particles do adopt a quasi-spherical shape without the presence of facets and edges in agreement with TEM observations (see Fig. 2a). Nevertheless, the energy analysis shows a strong surface heterogeneity. There is a difference of about 0.8 eV between the most energetic and the least energetic surface atoms, compared to a difference of about 0.6 eV in the solid state between vertices and facets {111}. This unexpected presence in the liquid state of highly energetic surface atoms whose weight decreases with increasing size (cf. Fig. 4b) is at the origin of the strong variation of γ with size, as in the solid state. The determination of the statistics of these sites as a function of size and temperature remains to be done. As proposed in case of solid

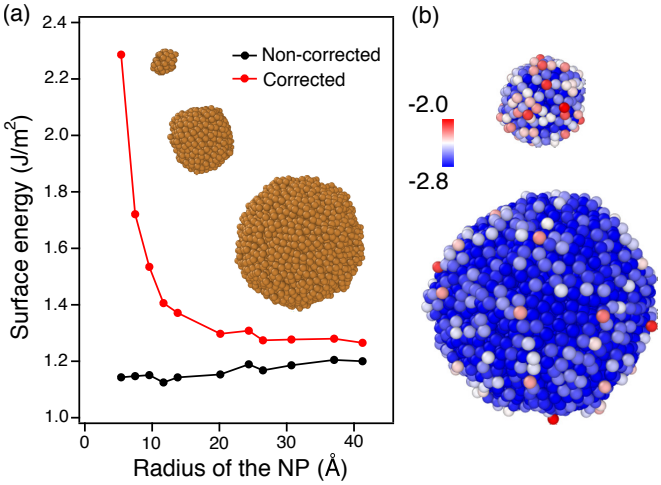

FIG. 4. (a) Calculated surface energies for liquid Cu NPs as a function of size within a spherical approximation and corrected spherical approximation. (b) Analysis of the local energies on surface of liquid NPs containing 561 and 5083 atoms. Energies are in eV.

NPs, this result therefore suggests that a heterogeneous surface necessarily tends to a variation in the value of γ.

Based on both numerical simulations and analytical developments, this study explains the origin of the disagreements regarding the evolution of the surface energy with the size of the NPs [19–24]. A strong dependence is obtained when the exact surface of the NP is considered, which is possible for simple forms. In contrast, using the classical spherical approximation, we obtain a surface energy that is almost independent of the size of the NP. If we correct the classical spherical approximation by taking into account the specific contribution of the surface atoms, we obtain a very good agreement with the exact calculation within one morphological factor. This result is particularly useful for dealing with liquid NPs, for which the exact surface area can hardly be calculated. How then can we explain the success of thermodynamic or kinetic approaches that use the classical spherical approximation and that reproduce well the experimental data, while neglecting the variation of γ with size [3–8]? The answer is that they rely on the expression of the chemical potential which involves the product γA and where the excess energy of the NP is considered to be localised at the surface (and does not contain core contributions as for the icosahedron). In these approaches, it is therefore essential to respect the consistency of the calculations of γ and A. This product can be evaluated either by considering the exact value of the surface area A and the exact variation of γ with size, or by considering the value of A given by the classical spherical approximation and the value of γ consistent with this calculation of A, namely a constant value equal to that of a semi-infinite bulk. In this latter case, even if the variations of γ and A are not exact, the product is correct explaining the success of thermodynamic or kinetic approaches based on the classical spherical approximation. This work therefore represents a significant achievement on an essential but difficult to define physical property at the nanoscale while proposing simple approaches to improve the thermodynamic and kinetic models developed so far in the future.

The support from the French research funding agency (ANR) under Grant No. 18-CE09-0014-01 (GIANT) is gratefully acknowledged. The authors are grateful to Région Ile de France for convention SESAME E1845 for the support of the JEOL electron microscope installed at Universit Paris. J.N. acknowledges funding from the French National Research Agency through the TOTEM project, Grant Number ANR-17-CE07-0031. H.A and B.L thank F. Ducastelle for fruitful discussions.

* hakim.amara@onera.fr

[1] L.-B. He, L. Zhang, L.-P. Tang, J. Sun, Q.-B. Zhang, and L.-T. Sun, "Novel behaviors/properties of nanometals induced by surface effects," Materials Today Nano **1**, 8–21 (2018).
[2] L. Vitos, A.V. Ruban, H.L. Skriver, and J. Kollár, "The surface energy of metals," Surf. Sci. **411**, 186 – 202 (1998).
[3] G. Wulff, "Zur Frage der Geschwindigkeit des Wachsthums und der Auflösung der Krystallflächen," Z. Kristallogr. **34**,

449 (1901).
[4] R. Kaishew, Comm. Bulg. Acad. Sci. **1**, 100 (1950).
[5] C. R. Henry, "Morphology of supported nanoparticles," Prog. Surf. Sci. **80**, 92 (2005).
[6] D. Alloyeau, G. Prévot, Y. Le Bouar, T. Oikawa, C. Langlois, A. Loiseau, and C. Ricolleau, "Ostwald ripening in nanoalloys: When thermodynamics drives a size-dependent particle composition," Phys. Rev. Lett. **105**, 255901 (2010).
[7] G. Prévot, N. T. Nguyen, D. Alloyeau, C. Ricolleau, and J. Nelayah, "Ostwald-driven phase separation in bimetallic nanoparticle assemblies," ACS Nano **10**, 4127–4133 (2016).
[8] A. Chmielewski, J. Meng, B. Zhu, Y. Gao, H. Guesmi, H. Prunier, D. Alloyeau, G. Wang, C. Louis, L. Delannoy, P. Afanasiev, C. Ricolleau, and J. Nelayah, "Reshaping dynamics of gold nanoparticles under H_2 and O_2 at atmospheric pressure," ACS Nano **13**, 2024–2033 (2019).
[9] Ph. Buffat and J-P. Borel, "Size effect on the melting temperature of gold particles," Phys. Rev. A **13**, 2287–2298 (1976).
[10] D. Alloyeau, C. Ricolleau, C. Mottet, T. Oikawa, C. Langlois, Y. Le Bouar, N. Braidy, and A. Loiseau, "Size and shape effects on the order-disorder phase transition in CoPt nanoparticles." Nat. Mater. **8**, 940–6 (2009).
[11] L. Delfour, J. Creuze, and B. Legrand, "Exotic behavior of the outer shell of bimetallic nanoalloys," Phys. Rev. Lett. **103**, 205701 (2009).
[12] Y. Magnin, A. Zappelli, H. Amara, F. Ducastelle, and C. Bichara, "Size dependent phase diagrams of nickel-carbon nanoparticles," Phys. Rev. Lett. **115**, 205502 (2015).
[13] F. T. Rabouw and C. De Mello Donega, "Excited-state dynamics in colloidal semiconductornanocrystals." Top Curr Chem (Z) **374**, 58 (2016).
[14] D. Guo, G. Xie, and J. Luo, "Mechanical properties of nanoparticles: basics and applications," J. Phys. D: Appl. Phys. **47**, 013001 (2013).
[15] K. K. Nanda, A. Maisels, F. E. Kruis, H. Fissan, and S. Stappert, "Higher Surface Energy of Free Nanoparticles," Phys. Rev. Lett. **91**, 106102 (2003).
[16] A. Chmielewski, J. Nelayah, H. Amara, J. Creuze, D. Alloyeau, G. Wang, and C. Ricolleau, "Direct Measurement of the Surface Energy of Bimetallic Nanoparticles : Evidence of Vegard's Rulelike Dependence," Phys. Rev. Lett. **120**, 025901 (2018).
[17] A. Perini, G. Jacucci, and G. Martin, "Interfacial contribution to cluster free energy," Surf. Sci. **144**, 53 – 66 (1984).
[18] T. P. Martin, T. Bergmann, H. Goehlich, and T. Lange, "Shell structure of clusters," J. Phys. Chem. **95**, 6421–6429 (1991).
[19] E. Müller, W. Vogelsberger, and H.-G Fritsche, "The dependence of the surface energy of regular clusters and small crystallites on the particle size," Cryst. Res. Technol. **23**, 1153–1159 (1988).
[20] B. Medasani, Y. H. Park, and I. Vasiliev, "Theoretical study of the surface energy, stress, and lattice contraction of silver nanoparticles," Phys. Rev. B **75**, 235436 (2007).
[21] S. Xiong, W. Qi, Y. Cheng, B. Huang, M. Wang, and Y. Li, "Modeling size effects on the surface free energy of metallic nanoparticles and nanocavities," Phys. Chem. Chem. Phys. **13**, 10648–10651 (2011).
[22] Y. Yao, Y. Wei, and S. Chen, "Size effect of the surface energy density of nanoparticles," Surf. Sci. **636**, 19–24 (2015).
[23] X. B. Jiang, B. B. Xiao, X. Y. Gu, and X. H. Zhang, "Modeling the effects of size and surface broken bond on surface energy of nanocrystals," Thin Solid Films **640**, 67–72 (2017).
[24] B. Molleman and T. Hiemstra, "Size and shape dependency of the surface energy of metallic nanoparticles: Unifying the atomic and thermodynamic approaches," Phys. Chem. Chem. Phys. **20**, 20575–20587 (2018).
[25] V. Rosato, M. Guillopé, and B. Legrand, "Thermodynamical and structural properties of f.c.c. transition metals using a simple tight-binding model," Philos. Mag. A **59**, 321 (1989).
[26] J. Creuze, I. Braems, F. Berthier, C. Mottet, G. Tréglia, and B. Legrand, "Model of surface segregation driving forces and their coupling," Phys. Rev. B **78**, 075413 (2008).
[27] F. Ducastelle, "Module élastique des métaux de transition," J. Phys. (Paris) **31**, 1055 (1970).
[28] D Frenkel and B. Smith, Understanding Molecular Simulation (Academic Press: London, 2002).
[29] S.W. Ip and J.M. Toguri, "The equivalency of surface tension , surface energy and surface free energy," Journal of Materials Science **29**, 688–692 (1994).
[30] P. Müller and A. Saúl, "Elastic effects on surface physics," Surf. Sci. Rep. **54**, 157 – 258 (2004).
[31] S. Ali, V. S. Myasnichenko, and E. C. Neyts, "Size-dependent strain and surface energies of gold nanoclusters," Phys. Chem. Chem. Phys. **18**, 792–800 (2016).
[32] Y. Wei and S. Chen, "Size-dependent surface energy density of spherical face-centered-cubic metallic nanoparticles," J. Nanosci. Nanotechnol. **15**, 9457–9463 (2015).
[33] D. Holec, P. Dumitraschkewitz, D. Vollath, and F. D. Fischer, "Surface energy of Au nanoparticles depending on their size and shape," Nanomaterials **10**, 484 (2020).

SUPPLEMENTARY MATERIAL OF : IS THERE REALLY A SIZE EFFECT ON THE SURFACE ENERGY OF NANOPARTICLES ?

Sec. I. Methodology

Within the tight-binding (TB) framework [1, 2], the total energy of an atom n is splitted in two parts, a band structure term that describes the formation of an energy band when atoms are put together and a repulsive term that empirically accounts for the ionic and electronic repulsions : $E^n_{tot} = E^n_{band} + E^n_{rep}$. The total energy of the system containing N atoms, E_{tot}, then writes $E_{tot} = \sum_{n=1,N} E^n_{tot}$. The band energy, E^n_{band} is given by :

$$E^n_{band} = -\sqrt{\sum_{m\neq n} \xi^2 \exp\left[-2q(\frac{r_{nm}}{r^0} - 1)\right]} \qquad (8)$$

and the repulsive contribution, E^n_{rep}, is chosen to have a pairwise Born-Mayer form :

$$E^n_{rep} = \sum_{m\neq n} A \exp\left[-p(\frac{r_{nm}}{r^0} - 1)\right] \qquad (9)$$

with r_{nm} the distance between atoms at sites n and m and r^0 corresponds to the equilibrium distance between first neighbors in the pure metal. ξ is the effective hopping integral between atoms. The parameters (ξ, A, q and p) used in this study are fitted to reproduce several bulk physical properties. More details concerning the fitting procedure can be found in our previous works dealing with the structural and thermodynamic properties of metallic nanoparticles [3, 4]. This atomic interaction model is implemented in a Monte Carlo (MC) code in the canonical ensemble, based on the Metropolis algorithm, which allows to relax the structures at finite temperature [5]. In the canonical ensemble, MC trials correspond to random displacements. The average quantities are calculated over 10^6 MC macrosteps, a similar number of macrosteps being used to reach equilibrium. A MC macrostep corresponds to N propositions of random atomic displacement, N being the total number of atoms of the cluster. Such approach is perfectly adapted to deal with large systems and to reproduce the main energetic properties of transition and noble metals.

Sec. II. Energy profiles along the radius of solid and liquid NPs

In Figure S1, we present the energy profiles along the radius of the different nanoparticles (147, 923 and 5083 atoms) in solid and liquid states. Such an analysis is made possible by the calculation of local energies derived directly from the TB model. Interestingly, we can clearly

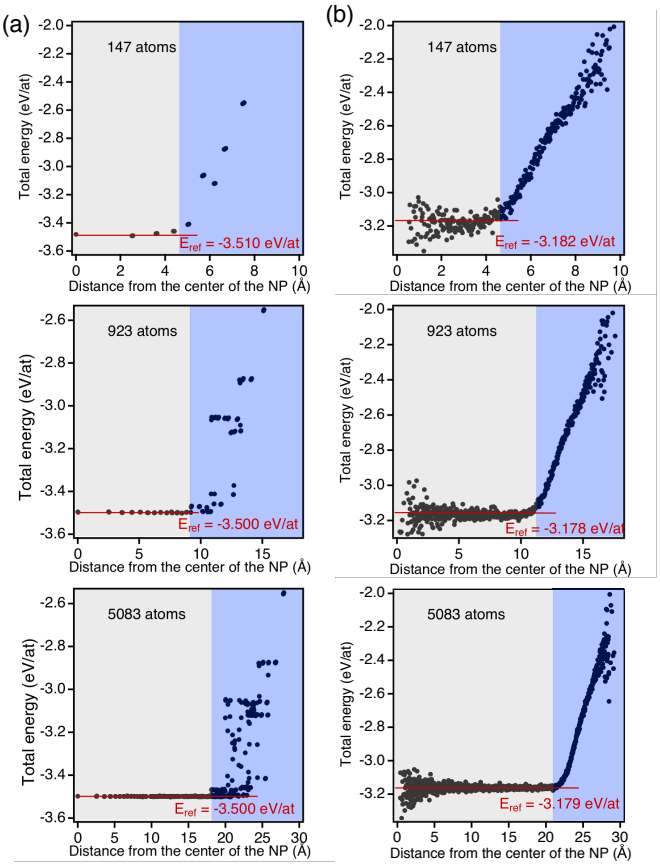

FIG. S1. Energy profiles along the radius of NPs containing 147, 923 and 5083 atoms (from top to bottom). Left : solid NPs (T=5 K) and right : liquid NPs (T=1500 K). The grey and blue areas represent the core and surface atoms, respectively.

identify two populations, i.e. core (grey area) and surface atoms (blue area). In case of solid NPs, the first corresponds to the core atoms which have energies around -3.50 eV/atom. The second population corresponds to surface atoms which are less stable and have energies reaching -2.60 eV/atom. The discontinuous aspect of the curve is mainly due to the layer structure of solid NP giving rise to this type of profile. For liquid NPs, the energy profiles along the particle are obviously more continuous. Here again, two populations of atoms are observed. The slice views shown in Figure S2 for solid and liquid NPs provide a direct insight into the distribution within the nanoparticle and confirms the presence of two populations where the excess energy is located at the surface.

Consequently, E_{ref} is simply the average energy of atoms identified in core position whatever the state of the NPs. In principle, it would be relevant to determine a different core energy for all sizes of NP. However, as the variation is very small (less than 10 meV/atom between Cu_{147} and Cu_{5083}), we choose

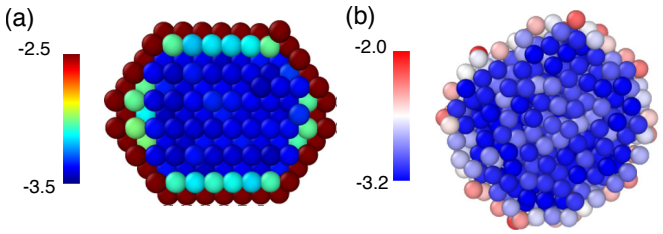

FIG. S2. Slice views showing the presence of core and surface populations for NPs containing 923 atoms in (a) solid and (b) liquid states. In case of solid NP, the contribution of subsurface atoms can be identified. Energies are in eV.

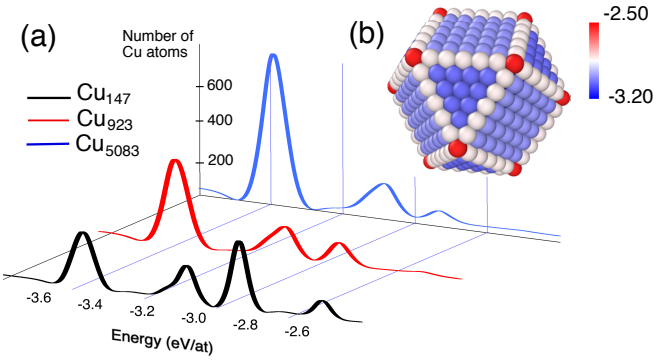

FIG. S3. (a) Analysis of the local energies in a histogram form for Cu solid NPs containing 147, 923 and 5083 atoms at 5K. For the sake of clarity, the values for the number of atoms in case of the NP_{147} have been increased by a factor of 10. (b) Analysis of the local energies on surface sites of solid Cu_{923} NP where different populations can be identified according to the following hierarchy : $E_f < E_e < E_v$. Note that the distinction between the different facets ({111} and {100}) is not visible at this scale. Energies are in eV/at.

to determine E_{ref} from the largest NP where the plateau corresponding to the core atoms is more clearly defined. In case of solid NP, E_{ref} is equal to -3.50 eV/at for solid NP which is exactly the total energy of a face-centered cubic bulk Cu in our TB model. In case of liquid NPs, E_{ref} is equal to -3.18 eV/at and corresponds to an infinite system in the liquid state at 1500 K.

Sec. III. Analysis of the local energies in solid nanoparticles

As an example, we plot the histogram of local energies for Cu NPs with total number of atoms, N = 147, 923 and 5083 atoms. Different populations of atoms can be identified (Fig S3a). The energies lie between -3.6 and -3.4 eV/atom are due to the bulk atoms which have 12 neighbors. The second population corresponds to the surface atoms which energies are below -3.2 eV/atom. As expected, the contribution of surface atoms decreases as the cluster size increases from Cu_{147} to Cu_{5083}. Moreover, a local analysis presented in Fig. S3b provides a spatial representation of the different surface sites with the following hierarchy : $E_{\{111\}} < E_{\{100\}} < E_e < E_v$. This result is not surprising since it is directly related to the coordination number (Z_i) of each site. The larger Z_i is, the higher the cohesion energy is. Finally, it is particularly interesting to note that local energies are independent on the size and remain constant whatever the nanoparticle under consideration.

Sec. IV. Calculation of surface energy from the exact definition of the surface area: $\gamma_{cubo}^{exact}(k)$

A cuboctahedral NP with k shells contains 12 vertices (v), 24(k-1) atoms in edges (e), 6(k-1)^2 and 4(k-2)(k-1) atoms on {100} and {111} facets (f), respectively. The total number of atoms $N(k)$, the volume $V(k)$ and the surface $S(k)$ are given by the following equations :

$$N(k) = \frac{10}{3}k^3 + 5k^2 + \frac{11}{3}k + 1 \tag{10}$$

$$V(k) = \frac{5\sqrt{2}}{3}(kd)^3 \tag{11}$$

$$S(k) = 2(3+\sqrt{3})(kd)^2 \tag{12}$$

In this section, we detail the analytical calculation of the surface energy which is written as follows:

$$\gamma_{cubo}(k) = \frac{\sum_i n_i \gamma_i}{A}, \tag{13}$$

γ_i represents the local excess energy for each surface site i ($i = v, e, f$) defined as $E_i - E_{ref}$. As for the surface area A, different approaches are possible. Here, A is considered as the exact surface $S(k)$ of the cuboctahedral nanoparticle. According to Eq. 13 and precise identification of surface sites, the surface energy is given by :

$$\gamma_{cubo}^{exact}(k) = \frac{12\gamma_v + 24(k-1)\gamma_e}{2k^2d^2(3+\sqrt{3})} + \frac{6(k-1)^2\gamma_{100} + 4(k-2)(k-1)\gamma_{111}}{2k^2d^2(3+\sqrt{3})}$$

From this we get :

$$\gamma_{cubo}^{exact}(k) = \frac{3\gamma_{100} + 2\gamma_{111}}{d^2(3+\sqrt{3})} + \frac{1}{d^2(3+\sqrt{3})} \times \left[\frac{6}{k}(2\gamma_e - \gamma_{100} - \gamma_{111}) + \frac{6\gamma_v - 12\gamma_e + 3\gamma_{100} + 4\gamma_{111}}{k^2}\right]$$

By limiting to the first-order Taylor approximation of $\gamma_{cubo}^{exact}(k)$, we obtain :

$$\gamma_{cubo}^{exact} \approx \gamma_{\infty}^{exact} + \frac{6\left[2\gamma_e - \gamma_{100} - \gamma_{111}\right]}{kd^2(3+\sqrt{3})}$$
$$\gamma_{\infty}^{exact} = \frac{3\gamma_{100} + 2\gamma_{111}}{d^2(3+\sqrt{3})}$$

Sec. V. Synthesis and TEM observations of solid and liquid NPs

The temperature serie of Transmission Electron Microscopy (TEM) images of the Cu NPs was acquired using a JEOL JEM-ARM200F spherical aberration corrected electron microscope equipped with a cold field emission gun operated at 80 kV here and a ultrafast Gatan OneView camera. For *in situ* TEM heating, we used a slightly modified version of the Atmosphere TEM environmental gas cell from Protochips Inc. with high temperature heating capabilities up to 1273 K [6].

The Cu NPs were synthesized by alternated pulsed laser deposition (PLD) technique in a high vacuum chamber at 10^{-5} Pa according to an experimental procedure detailed in [7]. The NPs was carried out directly on the 50-nm thick electron transparent silicon nitride membrane of the small heating E-chip that composes the Protochips gas cell. The nominal thickness of metal deposited was fixed at 2 nm and the SiN substrate was held at 723 K during metal deposition in order to obtain NPs with diameter below 10 nm. TEM observations were performed in vacuum with the SiN membrane of the larger E-chip of the gas cell removed.

Sec. VI. Calculation of the atomic density, ρ

In this section, we present the different approaches to calculate the atomic density for NPs, an important quantity which is taken into account in the γ calculation.

• Infinite system

In case of bulk, there is no particular difficulty since it can be straightforward determined from a face-centered cubic structure of lattice parameter a containing four atoms per cell. As a result, the atomic density of a bulk system is given by the following equation :

$$\rho_{\infty} = \frac{\sqrt{2}}{d^3}, \tag{14}$$

where d corresponds to the equilibrium distance between first neighbors in pure metals. Knowing that the lattice parameter of Cu is equal to 3.62 Å, we obtain $\rho \simeq 0.084$ atom/Å^3. In case of simulations at 1500 K, thermal expansion is taken into account leading to $\rho \simeq 0.076$ atom/Å^3. While this calculation seems trivial for an infinite volume, it has been ignored when using the spherical approximation in nanoparticles in literature.

• Nanoparticle

Atomic density from the total number of atoms $N(k)$

In case of a cuboctahedron NP, the number of atoms $N(k)$ and the volume $V(k)$ are known exactly. If we do not distinguish between core and surface sites and if we apply the following relation $\rho(k) = N(k)/V(k)$, the atomic density is simply given by :

$$\rho(k) = \frac{10k^3 + 15k^2 + 11k + 3}{5\sqrt{2}(kd)^3}$$

By limiting to the first-order Taylor expansion of $\rho(k)$, we obtain :

$$\rho(k) \approx \rho_{\infty}\left(1 + \frac{3}{2k}\right)$$

The fact that the atomic density of the NP is different from that of the bulk system before any relaxation clearly shows that the formula $\rho(k) = N(k)/V(k)$ should be corrected by differentiating the contribution of each type of site.

Atomic density by distinguishing between surface and bulk atoms

Let us consider $N_{eff}(k)$ the number of atoms in the NP where surface atoms $N_{surf}(k)$, counting for half, are removed : $N_{eff}(k) = N(k) - N_{surf}(k)/2$ where :

$$N_{surf}(k) = 6(k-1) + 4(k-2)(k-1) + 24(k-1) + 12$$

By limiting to the second-order Taylor expansion of $\rho(k) = N_{eff}(k)/V(k)$, we obtain :

$$\rho(k) \approx \rho_{\infty}\left(1 + \frac{11}{10k^2}\right) \tag{15}$$

In this case, the atomic density is equal to that of the bulk system at the first order.

This simple calculation on the cuboctahedron shows that it is essential to specifically take into account the contribution of the surface atoms to correctly obtain the atomic density of a nanoparticle. This is particularly useful and crucial when using the spherical approximation for NPs to calculate γ.

Sec. VII. Calculation of surface energy from the spherical approximation of the surface: $\gamma_{cubo}^{sa}(k)$ and $\gamma_{cubo}^{csa}(k)$

Spherical approximation

To determine the radius of a NP in the classical spherical approximation (sa), we use the relation $N = \rho V$ considering ρ_∞ the density of the infinite system and $N(k)$ the total number of atoms of the NP, without discriminating the contribution of core and surface atoms. As a result,

$$R^{sa}(k) = \left(\frac{3d^3N(k)}{4\pi\sqrt{2}}\right)^{1/3}$$

Knowing $N(k)$, the surface area within the spherical approximation is noted S^{sa} and can be expressed as :

$$S^{sa}(k) = 4\pi d^2 \left(\frac{3}{4\pi\sqrt{2}}\right)^{2/3} \times \left[1 + \frac{k}{3}(10k^2 + 15k + 11)\right]^{2/3} \quad (16)$$

From $R^{sa}(k)$ and $S^{sa}(k)$:

$$\gamma^{sa}_{cubo}(k) = \left(1 - \frac{1}{k} + \frac{31}{60}k^2\right) \times \left(\frac{1}{25\pi}\right)^{2/3} \times \left[(3\gamma_{100} + 2\gamma_{111}) + \frac{6}{k}(2\gamma_e - \gamma_{100} - \gamma_{111}) + \frac{6\gamma_v - 12\gamma_e + 3\gamma_{100} - 4\gamma_{111}}{k^2}\right]$$

By limiting to the first-order Taylor expansion of $\gamma^{sa}_{cubo}(k)$, we obtain :

$$\gamma^{sa}_{cubo}(k) \approx \gamma^{sa}_\infty + \frac{6\left[2\gamma_e - (3/2)\gamma_{100} - (4/3)\gamma_{111}\right]}{kd^2(25\pi)^{1/3}}$$

$$\gamma^{sa}_\infty = \frac{3\gamma_{100} + 2\gamma_{111}}{d^2(25\pi)^{1/3}},$$

It can be noted that in a simple manner the following relationship can be obtained :

$$\gamma^{sa}_\infty \approx 1.10\gamma^{exact}_\infty$$

Corrected spherical approximation

To correct the classical spherical approximation, we now distinguish between the contribution of core and surface atoms using $N^{eff}(k)$. A second-order Taylor expansion of $N^{eff}(k)$ leads to :

$$N^{eff}(k) \approx N(k)\left(1 - \frac{3}{2k} + \frac{9}{4k^2}\right)$$

Using this relation, we get :

$$R^{csa}(k) \approx \left[\frac{3}{4\pi\rho_\infty}N(k)\left(1 - \frac{3}{2k} + \frac{9}{4k^2}\right)\right]^{1/3}$$

$$S^{csa}(k) \approx 4\pi\left[\frac{3}{4\pi\rho_\infty}N(k)\left(1 - \frac{3}{2k} + \frac{9}{4k^2}\right)\right]^{2/3} \quad (17)$$

From the definition of $S^{sa}(k)$ (Eq. 16), $S^{csa}(k)$ can be written :

$$S^{csa}(k) \approx S^{sa}(k)\left(1 - \frac{3}{2k} + \frac{9}{4k^2}\right)^{2/3},$$

leading to the following relationship between $S^{csa}(k)$ and $S^{sa}(k)$ by limiting to the first-order Taylor expansion :

$$S^{csa}(k) \approx S^{sa}(k)\left(1 - \frac{1}{k}\right). \quad (18)$$

As seen in this equation, the corrected spherical approximation thus leads to a decrease in surface area relative to that of the spherical approximation.

In the following, we note $\gamma^{csa}_{cubo}(k)$ the surface energy obtained from the corrected spherical approximation. Considering previous equations, we simply get :

$$\gamma^{csa}_{cubo}(k) \approx \gamma^{sa}_{cubo}(k)\left(1 + \frac{1}{k}\right). \quad (19)$$

Moreover, from the initial definition of $\gamma^{sa}_{cubo}(k)$ and by limiting Eq. 19 to the first-order Taylor expansion of $\gamma^{csa}_{cubo}(k)$, we obtain :

$$\gamma^{csa}_{cubo}(k) = \frac{1}{d^2(25\pi)^{(1/3)}}\left[3\gamma_{100} + 2\gamma_{111} + \frac{6}{k}(2\gamma_e - \gamma_{100} - \gamma_{111})\right] \approx 1.10\left(\gamma^{exact}_\infty + \frac{6(2\gamma_e - \gamma_{100} - \gamma_{111})}{kd^2(3+\sqrt{3})}\right) \approx 1.10\gamma^{exact}_{cubo}(k) \quad (20)$$

The corrected spherical approximation is in very good agreement with the exact calculation with a constant form factor coming from the relation: $S^{csa}(k) = (1/1.10)S(k)$. Note that the value of 1.10 depends on the metal element.

Calculations of the radius for solid and liquid nanoparticles

Depending on its degree of accuracy, the spherical approximation gives rise to two calculations of radii in case of solid NPs, namely R^{sa} and R^{csa}. As seen in Table II, the difference is most significant for small NPs.

N	55	147	309	561	923	2869	5083	6525	10179	17885	24739
R^{sa}	5.3	7.4	9.5	11.6	13.7	20.1	24.3	26.4	30.7	37.0	41.3
R^{csa}	3.8	6.1	8.3	10.4	12.6	19.0	23.2	25.3	29.6	35.9	40.2

TABLE II. For each NP containing N atoms, R is obtained within the spherical approximation and corrected spherical approximation in solid state. Values are given in Å.

* hakim.amara@onera.fr

[1] V. Rosato, M. Guillopé, and B. Legrand, "Thermodynamical and structural properties of f.c.c. transition metals using a simple tight-binding model," Philos. Mag. A **59**, 321 (1989).

[2] J. Creuze, I. Braems, F. Berthier, C. Mottet, G. Tréglia, and B. Legrand, "Model of surface segregation driving forces and their coupling," Phys. Rev. B **78**, 075413 (2008).

[3] L. Delfour, J. Creuze, and B. Legrand, "Exotic behavior of the outer shell of bimetallic nanoalloys," Phys. Rev. Lett. **103**, 205701 (2009).

[4] A. Chmielewski, J. Nelayah, H. Amara, J. Creuze, D. Alloyeau, G. Wang, and C. Ricolleau, "Direct Measurement of the Surface Energy of Bimetallic Nanoparticles : Evidence of Vegard's Rulelike Dependence," Phys. Rev. Lett. **120**, 025901 (2018).

[5] D Frenkel and B. Smith, Understanding Molecular Simulation (Academic Press: London, 2002).

[6] A. Chmielewski, C. Ricolleau, D. Alloyeau, G. Wang, and J. Nelayah, "Nanoscale temperature measurement during temperature controlled in situ TEM using Al plasmon nanothermometry," Ultramicroscopy **209**, 112881 (2020).

[7] H. Prunier, J. Nelayah, C. Ricolleau, G. Wang, S. Nowak, A.-F. Lamic-Humblot, and D. Alloyeau, "New insights into the mixing of gold and copper in a nanoparticle from a structural study of Au-Cu nanoalloys synthesized via a wet chemistry method and pulsed laser deposition," Phys. Chem. Chem. Phys. **17**, 28339–28346 (2015).